THE ASTROPHYSICAL JOURNAL, 425:L89–L92, 1994 April 20

A ROCKET-BORNE OBSERVATION OF THE FAR-INFRARED SKY AT HIGH GALACTIC LATITUDE

M. KAWADA,[1] J. J. BOCK,[2] V. V. HRISTOV,[2] A. E. LANGE,[2] H. MATSUHARA,[1] T. MATSUMOTO,[1] S. MATSUURA,[1] P. D. MAUSKOPF,[2] P. L. RICHARDS,[2] AND M. TANAKA[1]

Received 1993 October 13; accepted 1994 February 7

ABSTRACT

We have measured the surface brightness of the far-infrared sky at $\lambda = 134$, 154, and 186 μm at high Galactic latitude using a liquid-He–cooled, rocket-borne telescope. The telescope scanned over a $5° \times 20°$ region which includes infrared cirrus, high-latitude molecular clouds, the starburst galaxy M82, and the H I Hole in Ursa Major, a region with uniquely low H I column density. The measured brightness at 134, 154, and 186 μm is well correlated with the 100 μm brightness measured by *IRAS* and, in regions excluding molecular clouds, with H I column density. The spectrum of the component correlated with H I is well fitted by a gray-body spectrum with a temperature of $16.4(+2.3/-1.8)$ K, assuming an emissivity proportional to λ^{-2}. Assuming a constant far-infrared dust emissivity per hydrogen nucleus, the ratio of the H_2 column density to the velocity-integrated CO intensity in the high-latitude molecular cloud is $N(H_2)/W_{CO} = (1.6 \pm 0.3) \times 10^{20}$ cm^{-2} (K km s^{-1})$^{-1}$. The residual brightness after subtracting the emission correlated with H I column density is $\lambda I_\lambda(154\ \mu\text{m}) = (1.4 \pm 0.6) \times 10^{-12}$ W cm^{-2} sr^{-1}, yielding an upper limit to the far-infrared extragalactic background radiation of $\lambda I_\lambda(154\ \mu\text{m}) < 2.6 \times 10^{-12}$ W cm^{-2} sr^{-1}.

Subject headings: dust, extinction — infrared: general — ISM: clouds

1. INTRODUCTION

The diffuse infrared background measured by the *Infrared Astronomical Satellite* (*IRAS*) is dominated by emission from the interplanetary dust (IPD) in the 12, 25, and 60 μm bands and emission from the interstellar dust (ISD) in the 100 μm band (Boulanger & Pérault 1988). At high Galactic latitude, "IR cirrus" was observed, which has a complex spatial distribution (Low et al. 1984). The brightness of the IR cirrus is well correlated with the column density of neutral hydrogen (H I) and is generally attributed to thermal emission from ISD with a temperature $T \sim 20$ K. In addition to these "local" sources of emission, several theories predict an extragalactic background radiation (EBR) due to the integrated light from distant galaxies. Some models suggest that primeval galaxies were obscured by dust and emitted a significant portion of their energy at far-infrared wavelengths. Detection of an EBR at far-infrared wavelengths would have important implications for an understanding of the early universe (Beichman & Helou 1991; Oliver, Rowan-Robinson, & Saunders 1992).

The detection of a far-infrared EBR requires absolute photometry using a cooled telescope in space. Rocket-borne experiments (for example, Matsumoto et al. 1988) and the DIRBE on *COBE* (Hauser et al. 1991) have established upper limits on the infrared EBR which are limited by the brightness of local sources of emission. More sensitive searches require careful modeling and subtracting of local sources of foreground emission. This paper describes a measurement of the distribution of ISD emission in a region at high Galactic latitude using a rocket-borne instrument with unprecedented sensitivity and provides a new upper limit on the far-infrared EBR.

2. INSTRUMENT

The instrument consisted of a 10 cm diameter Cassegrain telescope, a baffle system (Bock et al. 1994b), and a photometer, all cooled to 2 K by superfluid liquid helium. The photometer had five spectral channels separated by filters: three broad-band channels at 95, 134, and 186 μm and two narrow-band channels at 154 μm and 158 μm for observation of the fine-structure line of [C II] $^2P_{3/2} \rightarrow {}^2P_{1/2}$ at 157.7 μm. The results of the [C II] observation have been reported previously (Bock et al. 1993). The detectors, stressed and unstressed Ge:Ga photoconductors, were cooled to 0.9 K by a ^{4}He refrigerator (Bock et al. 1994a). The photocurrent was measured by a charge-integrating readout circuit. The small dark current ($\lesssim 30$ e$^-$ s^{-1}) and low readout noise (~ 60 e$^-$ for a 1 s integration) provided high sensitivity. The specifications of the instrument are summarized in Table 1. Further details are described in Matsuhara et al. (1994).

The instrument had a cold shutter to measure the instrument offset and a calibration lamp located behind the cold shutter to monitor the responsivity. The shutter and the calibration lamp were operated periodically during the laboratory and the rocket-borne measurements. The instrument was absolutely calibrated in the laboratory using a variable temperature blackbody source which partially filled the entrance aperture of the telescope, giving an effective emissivity of 0.036%. The incident intensity was varied over three orders of magnitude by controlling the temperature of the blackbody between 10 K and 30 K and in each channel included the intensity observed during the flight. Instrument emission was measured to be negligible. The accuracy of the relative and absolute calibration is estimated to be 10% and 20%, respectively.

3. OBSERVATION

The instrument was launched on the sounding rocket S-520-15 at 1:00 (Japanese Standard Time) on 1992 February 2 from

[1] Department of Astrophysics, Nagoya University, Nagoya 464, Japan.
[2] Department of Physics and Space Sciences Laboratory, University of California, Berkeley, CA 94720.

TABLE 1

SPECIFICATIONS OF THE FAR-INFRARED PHOTOMETER

λ_c[a] (μm)	$\Delta\lambda$[a] (μm)	Beam (ϕ_{HPBW})	Sensitivity: λI_λ[b] (pW cm^{-2} sr^{-1})
95.....	20	0°.5	6.7
134.....	13	0.5	0.2
154.....	1.5	0.65	0.6
186.....	24	0.5	0.3

[a] Median central wavelength and bandwidth for λI_λ = const.

[b] Sensitivity (1 σ) for a 1 s integration in the flight.

the Kagoshima Space Center of the Institute of Space and Astronautical Science (ISAS) in Japan. The payload was separated from the rocket motor at 60 s after launch and reached an apogee of 338 km at 293 s after launch. At 130 s after launch, a lid covering the telescope was opened, and observation began of the H I Hole, a region with a uniquely low H I column density, $\sim 5 \times 10^{19}$ cm^{-2} (Jahoda, Lockman, & McCammon 1990), that is ideal for an EBR search. The observation sequence, shown in Figure 1 of Bock et al. (1993), was as follows: from 130 s to 220 s, the telescope was pointed at the H I Hole, $(l, b) \sim (151°, 52°)$; from 220 s to 310 s, the telescope scanned along a triangular path through infrared cirrus, molecular clouds, and the starburst galaxy M82; from 310 s to 430 s, the telescope was pointed again at the H I Hole; from 430 to 480 s, the telescope was tilted to the horizontal to facilitate the recovery of the attitude control system; at 480 s, the instrument was separated from the rocket payload. Details are described in Matsuhara et al. (1994).

4. DATA REDUCTION

The time profile of the 134 μm data is plotted in Figure 1. The periodic dips correspond to the closings of the cold shutter, indicating zero signal level. Spikelike features just before each shutter closing correspond to emission from the calibration lamp superposed on the sky signal. A time-dependent, decreasing component of emission is present until 200 s. During the scanning observation, infrared cirrus, a molecular cloud (around 245 s) and M82 (at 291 s) are clearly detected. Although the telescope is pointed at the H I Hole, the signal gradually increases after 380 s. This increase is one order of magnitude larger than that expected from atmospheric O I emission (Grossmann & Offermann 1978). A similar phenomenon was seen in some channels of a near-infrared spectrometer which shared the focal plane (Matsuura et al. 1994). The observed increase is presumably due to emission from contaminants associated with the rocket motor. To minimize the

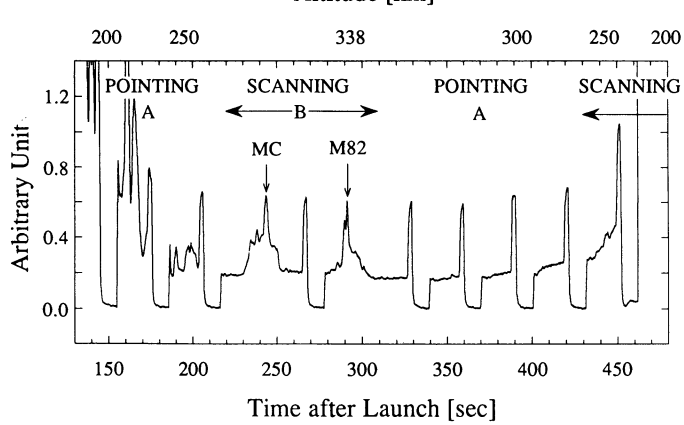

FIG. 1.—The time profile of the raw 134 μm data. The observation began 130 s after launch and continued until 480 s. MC and M82 indicate the observation of the molecular cloud and the starburst galaxy M82, respectively.

contribution of this emission, only the data between 210 s and 380 s after launch are used in the analysis. For these data, the variation of the signal at the H I Hole is less than 10%. We cannot exclude the possibility of a constant component of emission from contaminants.

The instrument offset is subtracted using the signal at the shutter closings. The response to the calibration lamp was stable during the flight for all channels. The response was within 5% of that measured in the laboratory at 154 μm and 158 μm, but it was significantly different from that measured in the laboratory at 95, 134, and 186 μm, by $(+25 \pm 12)$%, (-27 ± 1)%, and (-24 ± 2)%, respectively. We correct the absolute responsivity during the flight by the ratio of the signal from the calibration lamp observed in the laboratory and in the flight, but we include the discrepancy in the absolute responsivity at 95, 134, and 186 μm as a systematic error. The reliability of the absolute responsivity can be checked using the observation of the galaxy M82, which was observed at 134 μm and 154 μm. Using the responsivity normalized to the calibration lamp and including the uncertainty in our attitude determination and beam profile, the flux we observed is consistent with the observation of (D. Harper, 1992, private communication). The observations of M82 are compared in Table 2.

5. RESULTS AND DISCUSSION

5.1. *Galactic Far-Infrared Emission at High Galactic Latitude*

The distribution of the far-infrared continuum data is compared to *IRAS* 100 μm data (see *IRAS* Sky Survey Atlas

TABLE 2

EXPERIMENTAL RESULTS

λ (μm)	λI_λ[a] / *IRAS* $\lambda I_{100\,\mu m}$	λI_λ[a] / N(H I) (10^{-32} W sr^{-1})	H I RESIDUAL[a] (pW cm^{-2} sr^{-1})	M82 This work (10^{-15} W cm^{-2})	M82 Harper[b] (10^{-15} W cm^{-2})
134.....	$2.0^{+0.4}_{-0.9}$	$3.9^{+0.9}_{-1.7}$	$8.0^{+1.6}_{-3.5}$	4.0 ± 1.4	3.6 ± 0.9
154.....	$1.5^{+0.4}_{-0.3}$	$3.2^{+0.7}_{-0.8}$	$1.4^{+0.6}_{-0.6}$	$1.6^{+0.7}_{-0.4}$	2.5 ± 0.6
186.....	$1.5^{+0.4}_{-0.6}$	$3.0^{+0.6}_{-1.2}$	$2.4^{+0.5}_{-1.1}$	...	...

NOTE.—Estimation of errors is described in the text.

[a] Best linear-fit results for regions without CO emission.

[b] Calculated flux assuming a graybody spectrum with $n = 2$ and $T = 31.2$ K.

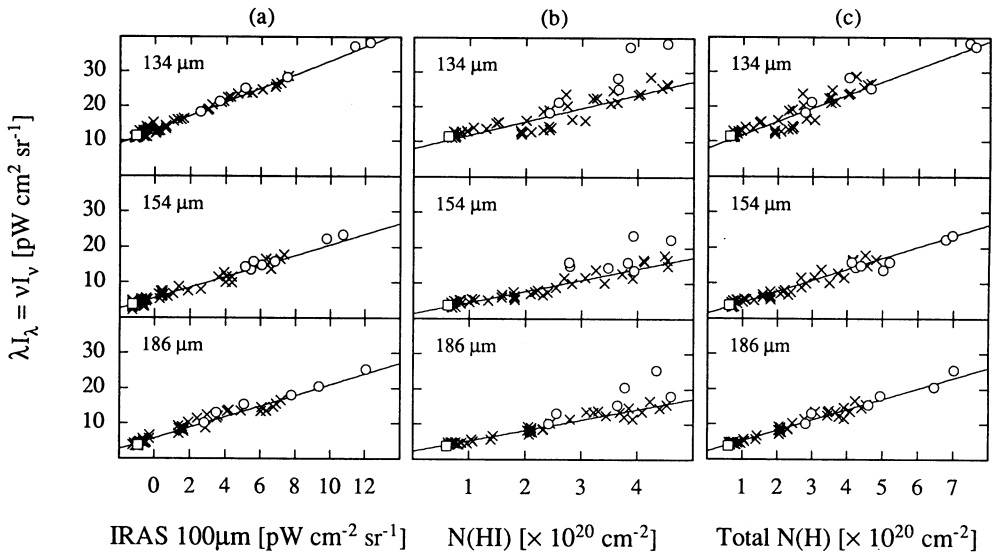

FIG. 2.—Point-to-point comparison between the observed intensity (134, 154, 186 μm) and (*a*) *IRAS* 100 μm intensity; (*b*) H I column density; and (*c*) total H column density, which is calculated from the relation $N(\mathrm{H}) = N(\mathrm{H\,I}) + 2[N(\mathrm{H_2})/W_{\mathrm{CO}}]W_{\mathrm{CO}}$ (see text). Open circles indicate regions with CO emission; crosses indicate regions where CO emission is absent. The data at the H I Hole is indicated by open squares. Lines in each panel indicate the best linear fit, excluding regions with CO emission. Statistical error bars are smaller than the size of the symbols.

1991), CO data (de Vries Heithausen, & Thaddeus 1987) and H I data (Dickey & Lockman 1990) in Figure 2. The 95 μm data are excluded from Figure 2 because of this poor sensitivity. Figure 2*a* shows the correlation with the *IRAS* 100 μm data, which has been convolved with the field of view of the photometer and corrected to the DIRBE calibration by multiplying by 0.72 (see Explanatory Supplement for the DIRBE Galactic Plane Maps 1993). Regions with velocity-integrated CO intensity W_{CO} greater than 0.1 K km s^{-1} ("CO regions") are indicated by open circles. The data at all wavelengths are well correlated with *IRAS* 100 μm emission. The solid lines in the figure indicate the best linear fit excluding the CO regions. The excellent fit suggests that the 100–200 μm emission originates primarily from the same source observed by *IRAS* at 100 μm. The CO regions fall along the same line, suggesting that the temperature and spectral index of the dust inside and outside of these low-column density CO clouds is similar. The spectrum of the *IRAS*-correlated component has a temperature $T = 16.6(+2.2/-1.7)$ K, if we assume an emissivity $\propto \lambda^{-2}$.

The correlations with the column density of neutral hydrogen are shown in Figure 2*b*. The column density of H I, including all velocities within $|v| < 250$ km s^{-1}, was averaged into 1° × 1° bins in Galactic longitude and Galactic latitude. The small difference between the lowest column density 5.3 × 10^{19} cm^{-2} in this data set and the minimum of 4.4 × 10^{19} cm^{-2} in Jahoda et al. (1990) is due to the 1° × 1° averaging (F. Lockman, 1993 private communication). There is a good correlation of the observed far-infrared intensity with H I column density, excluding the CO regions, as shown by the linear fits in Figure 2*b*. The spectrum of the H I–correlated component is shown in Figure 3 with filled and open squares for the column density at the H I Hole, $N(\mathrm{H\,I}) = 6 \times 10^{19}$ cm^{-2}. The 100 μm point (*open square*) was calculated from the *IRAS* 100 μm data corrected to the DIRBE calibration as described above. The spectrum of the H I–correlated component, including the *IRAS* 100 μm point, is similar to that of the *IRAS*-correlated component, giving a temperature $T = 16.4(+2.3/-1.8)$ K. This temperature is in good agreement with that measured at 140 μm and 240 μm in the outer Galaxy by DIRBE (Sodroski et al. 1994). The bolometric far-IR emission is $L_{\mathrm{FIR}} = (4.7 + 0.8/-1.3) \times 10^{-31}$ W (H I atom)$^{-1}$.

As shown in Figure 2*b*, the CO regions, where $W_{\mathrm{CO}} < 1$ K km s^{-1}, have a higher far-infrared intensity per H I atom than regions without CO emission. The excess brightness can be interpreted as emission from the dust associated with molecular hydrogen. We estimate the ratio of the column density of

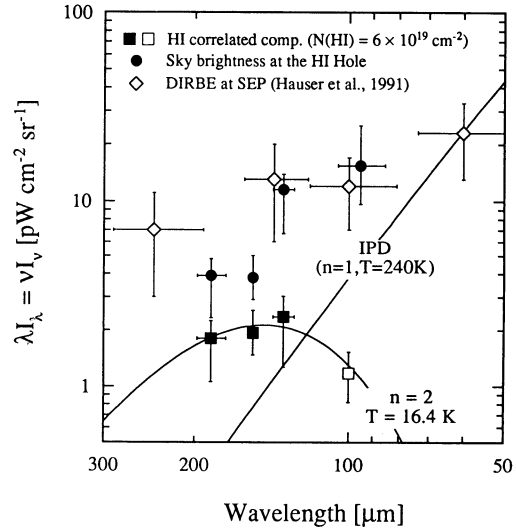

FIG. 3.—The brightness of the H I–correlated component observed by this experiment at 134, 154, and 186 μm (*filled square*) and by *IRAS* at 100 μm (*open square*), normalized to the column density of H I at the H I Hole [$N(\mathrm{H\,I}) = 6 \times 10^{19}$ cm^{-2}]. The solid line is the best-fit spectral model of $n = 2$, $T = 16.4$ K. Filled circles show the sky brightness observed at the H I Hole. The brightness of the south ecliptic pole (SEP) observed by DIRBE is plotted by open diamonds. For the purpose of illustration, we show an IPD model of $n = 1$ and $T = 240$ K normalized to the DIRBE 60 μm data point. Error bars in the figure include systematic error.

hydrogen molecules $N(H_2)$ to W_{CO} by assuming the same far-infrared emissivity for dust in regions with and without CO emission, as is suggested by the correlation with the *IRAS* 100 μm data. We find $N(H_2)/W_{CO} = (1.6 \pm 0.3) \times 10^{20}$ cm^{-2} (K km s^{-1})$^{-1}$, with no significant change between channels. This result is lower than that for the Galactic plane, 2.8×10^{20} cm^{-2} (K km s^{-1})$^{-1}$ (Bloemen et al. 1986), but is higher than that of de Vries et al. (1987), $(0.5 \pm 0.3) \times 10^{20}$ cm^{-2} (K km s^{-1})$^{-1}$, over a larger region of the same CO cloud. The difference between our result and that of de Vries et al. (1987) may be due to the small size of the CO regions we sampled. In Figure 2*c* we replace the horizontal axis with the total column density of hydrogen atoms, using the relation $N(H) = N(H\ I) + 2[N(H_2)/W_{CO}]W_{CO}$. The resulting plot indicates a good correlation between observed intensity and the total column density of hydrogen atoms in all channels for all observed regions.

5.2. *Other Emission Components*

The sky brightness measured at 154 μm and 186 μm at the H I Hole, shown in Figure 3 by filled circles, is significantly lower than that of the south ecliptic pole observed by DIRBE (Hauser et al. 1991). This result is consistent with the smaller H I column density at the H I Hole. The brightness at the H I Hole may be attributed to emission from ISD, IPD, EBR, and/or rocket-borne contamination. A simple model of IPD emission is plotted in Figure 3 assuming a graybody thermal spectrum with $n = 1$ and $T = 240$ K normalized to the DIRBE 60 μm data point. The sky brightness detected at 95 μm and 134 μm is much higher than can be accounted for by IPD and ISD emission. Rocket-borne contamination may account for the large signals in these channels. It is interesting to note that these two channels had pronounced time-dependent signals near the end of the flight, whereas the 154 μm and 186 μm data did not.

The intersection at $N(H\ I) = 0$ of the correlation with H I column density shown in Figure 2*b* gives an upper limit on the EBR. The brightness of the H I residual component at 154 μm and 186 μm, listed in Table 2, is smaller than upper limits previously reported (Boulanger & Pérault 1988). The upper limit on the EBR we derived, $\lambda I_\lambda(154\ \mu m) < 2.6 \times 10^{-12}$ W cm^{-2} sr^{-1}, is sufficiently small to exclude some high evolution models of IR galaxies, such as $\gamma = 4$ and $z_{max} > 3$ in Beichman & Helou (1991).

6. SUMMARY

We have observed the far-infrared sky at high Galactic latitude using a rocket-borne absolute photometer. We found:

1. The spectrum of emission from the ISD is similar in all regions observed, including low–column density CO clouds. The temperature is $T = 16.4(+2.3/-1.8)$ K, assuming emissivity $\propto \lambda^{-2}$.
2. The $N(H_2)/W_{CO}$ ratio of $(1.6 \pm 0.3) \times 10^{20}$ cm^{-2} (K km s^{-1})$^{-1}$ is derived for a high Galactic latitude cloud by comparison with H I and CO observations.
3. The brightness of the EBR at 154 μm is $\lambda I_\lambda(154\ \mu m) < 2.6 \times 10^{-12}$ W cm^{-2} sr^{-1}, which excludes some high evolution models of infrared galaxies.

We would like to thank J. Beeman, N. Hiromoto, A. Heithausen, H. Okuda, the staff at ISAS, machine shops at Nagoya University and University of California, Berkeley, and the Daiko Science Foundation. This work was supported by grants-in-aid from the Ministry of Education, Science, and Education in Japan (03249213, 03740128, and 04233215), Fellowships of the Japan Society for the Promotion of Science for Japanese Junior Scientists, David and Lucile Packard Foundation, and NASA grants NAGW-1352 and NGT-50771.

REFERENCES

Beichman, C. A., & Helou, G. 1991, ApJ, 370, L1
Bloemen, J. B. G., et al. 1986, A&A, 154, 25
Bock, J. J., et al. 1993, ApJ, 410, L115
Bock, J. J., Duband, L., Kawada, M., Matsuhara, H., Matsumoto, T., & Lange, A. E. 1994a, Cryogenics, in press
Bock, J. J., Lange, A. E., Matsuhara, H., Matsumoto, T., Onaka, T., & Sato, S. 1994b, Appl. Opt., submitted
Boulanger, F., & Pérault, M. 1988, ApJ, 330, 964
de Vries, H. W., Heithausen, A., & Thaddeus, P. 1987, ApJ, 319, 723
Dickey, J. M., & Lockman, F. J. 1990, ARA&A, 28, 215
Explanatory Supplement for the DIRBE Galactic Plane Maps. 1993
Grossmann, K. U., & Offermann, D. 1978, Nature, 276, 594
Hauser, M. G., et al. 1991, in AIP Conf. Proc. 222, After the First Three Minutes, ed. S. S. Holt, C. L. Bennett, & V. Trimble (AIP: New York), 161
IRAS Sky Survey Atlas. 1991
Jahoda, K., Lockman, F. J., & McCammon, D. 1990, ApJ, 354, 184
Low, F. J., et al. 1984, ApJ, 278, L19
Matsuhara, H., et al. 1994, PASJ, in press
Matsumoto, T., Hayakawa, S., Matsuo, H., Murakami, H., Sato, S., Lange, A. E., & Richards, P. L. 1988, ApJ, 329, 567
Matsuura, S., Bock, J. J., Kawada, M., Matsuhara, H., Matsumoto, T., Noda, M., & Tanaka, M. 1994, PASP, submitted
Oliver, S. J., Rowan-Robinson, M., & Saunders, W. 1992, MNRAS, 256, 15
Sodroski, T. J., et al. 1994, ApJ, in press